JCTC Journal of Chemical Theory and Computation

ARTICLE

pubs.acs.org/JCTC

Excited State Dynamics of the Green Fluorescent Protein on the Nanosecond Time Scale

Gabriella Jonasson,*[,†] Jean-Marie Teuler,[†] Germain Vallverdu,[‡] Fabienne Mérola,[†] Jacqueline Ridard,[†] Bernard Lévy,[†] and Isabelle Demachy*[,†]

[†]Laboratoire de Chimie-Physique, UMR8000, CNRS, Université Paris-Sud 11, 91405 Orsay Cedex, France

[‡]Equipe de Chimie-Physique, IPREM, UMR5254, Université de Pau et des Pays de l'Adour, 64000 Pau, France

Supporting Information

ABSTRACT: We have introduced a new algorithm in the parallel processing PMEMD module of the AMBER suite that allows MD simulations with a potential involving two coupled torsions. We have used this modified module to study the green fluorescent protein. A coupled torsional potential was adjusted on high accuracy quantum chemical calculations of the anionic chromophore in the first excited state, and several 15-ns-long MD simulations were performed. We have obtained an estimate of the fluorescence lifetime (2.2 ns) to be compared to the experimental value (3 ns), which is, to the best of our knowledge, the first theoretical estimate of that lifetime.

1. INTRODUCTION

Fluorescent proteins (FPs) of the green fluorescent protein (GFP) family are invaluable fluorescent markers in cell biology.[1−5] There is a huge number of mutants and homologues which all share the same overall structure (Figure 1) and general photophysical characteristics. Most of the brightly fluorescent FPs exhibit fluorescence emission on the nanosecond time scale while in solution or in denaturated (unfolded) proteins; the quantum yield of the chromophore is low (10^3 times smaller than in folded protein) and the fluorescence decay very fast (0.2−1.1 ps for the GFP anionic chromophore in water[6]). Besides, the diversity of fluorescence quantum yields exhibited by proteins carrying identical chromophores in the GFP superfamily[7] points to the decisive role of the protein architecture in controlling the chromophore radiationless decay.

Classical dynamics simulations based on a semiempirical Hamiltonian[8] or quantum dynamics studies[9,10] of the GFP excited S_1 chromophore in vacuo have established that fluorescence quenching occurs through torsion around the two central bonds linking the methylene group to each aromatic ring (τ and φ angles, see Figure 1) and that these torsions take place within a few picoseconds after excitation. It implies that the order of magnitude of the fluorescence lifetime (ns) observed in the folded proteins results from a hindrance of the torsion motions by the protein matrix. Obviously, this hindrance is not a massive steric locking of the motions since in most FPs the volume of the cavity around the chromophore may accommodate twisted geometries.[11,12] In fact, the constraints exerted by the protein have been scarcely studied.[9,11−14]

A thorough description of the chromophore−protein interaction is challenging because

(i) It requires a molecular dynamics (MD) calculation significantly longer than a nanosecond with the chromophore in the excited state. Quantum-mechanics/molecular-dynamics (QM/MD) methods would be ideal for such studies, and they have already been used to study the radiationless decay of dark states in photoswitchable proteins like asFP595[15] or Dronpa,[16] for which a much smaller simulation time is needed (1 and 20 ps). However, these methods are heavily computer-time-demanding and cannot be used presently to run simulations on the nanosecond time scale.

(ii) If one turns to classical force field MD simulations, nanosecond simulations become feasible, but one is then faced with a difficulty related to the interplay between the τ and φ torsions. Standard MD programs assume additive potentials, which, in that case, imply an energy minimum in the geometry where the two angles are twisted (the so-called "hula twist" geometry[17]) in complete contradiction with *ab initio* calculations.[18]

The aim of this work is to enable nanosecond-long MD simulations with a force field accounting for the interaction between the two torsions (2D force field). To that end, we need an analytical 2D potential. Such a potential has already been proposed,[19] but it is based on only a few *ab initio* energy values. Thus, we have first performed accurate *ab initio* calculations of the first excited state of the GFP chromophore on a tight grid of geometries. We have then fitted the energies using an algebraic expression depending on τ and φ, and finally we have introduced a new algorithm in the parallel processing PMEMD module in the AMBER suite[20] that allows MD simulations using a 2D force field. In section 2, we first describe the development of the coupled torsional potential $V(\tau,\varphi)$ (*ab initio* calculations, fitting procedure, and implementation in the AMBER suite); we then discuss the resulting 2D potential energy surface (PES) and the results obtained by MD simulations in vacuo using the 2D potential and finally analyze the accuracy and sensibility of this

Received: March 1, 2011
Published: April 28, 2011

ACS Publications © 2011 American Chemical Society

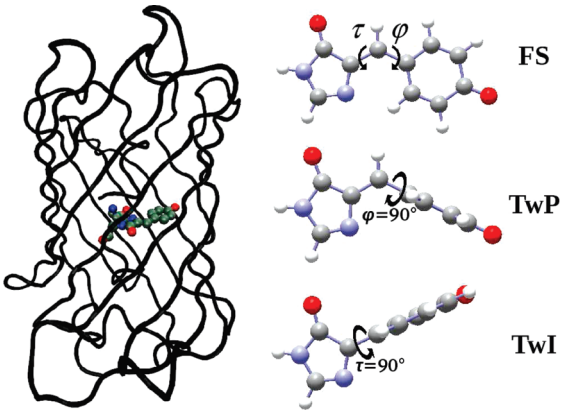

Figure 1. Left: GFP with the chromophore covalently bound to the central α-helix. Right: the anionic GFP *cis* chromophore model p-hydroxybenzylidene-imidazolinone (HBI) in three different geometries: the planar fluorescent state (FS) minimum ($\tau = \varphi = 0°$), the TwP geometry — twisted 90° around the phenol bridge bond — and the TwI geometry — twisted 90° around the imidazolinone bridge bond.

potential. In section 3, we report results from several 15-ns-long MD simulations of GFP and present a theoretical estimate of the fluorescence lifetime. All calculations were performed on the anionic chromophore—the species responsible for the green fluorescence.

2. COUPLED TORSIONAL POTENTIAL $V(\tau,\varphi)$

2.1. Quantum Chemical Method. We have determined the energy of the S_1 excited state of the anionic chromophore in different geometries at the SA2-CAS(4,3) (two state average-complete active space multiconfiguration self-consistent field[21] with a four electrons-three orbitals active space) level of theory with the 6-31G* basis set for geometry optimizations, followed by a single point PT2 (second-order perturbation theory) computation. The CASSCF and CASPT2 calculations have been performed here using the Gaussian[22] and Molpro[23] program packages, respectively. The anionic chromophore has been represented by the p-hydroxybenzylidene−imidazolinone (HBI) motif (Figure 1).

The CASSCF method is today a common choice for determining excited-state geometries of biological chromophores,[8,18,25,26] but some comments seem necessary on the specific choices of an active space with three orbitals and four electrons and of a two state average. In fact, it has been demonstrated[19] that an appropriate mesomeric description of the electronic wave function of molecules like the anionic GFP chromophore involves at least three structures: two structures P and I with a double bond either on CA2−CB2 or on CB2−CG2 (see Figure 6 in Appendix A for atom names) and a third structure B with an unpaired electron on CA2 and a second unpaired electron on CG2. Such mesomeric structures are found in systems with three orbitals and four electrons[27] or in bigger compounds like Brooker dyes.[28] Unless one of the bonds is lengthened,[27] the third structure B has a lower weight in the first two electronic states S_0 and S_1 compared to the weights of structures P and I (ref 19, Tables V, VI, VII); yet, structure B is required in order to couple P and I.

These three structures are properly taken into account in a CI with four electrons and three orbitals. Now, if one is interested in the first excited state S_1, one cannot just minimize the second root of the CI because then the energy of the ground state S_0, constructed with the same orbitals as S_1, increases, giving rise to a flip-flop between the two states. A more efficient approach consists of first minimizing the average of the energies of the two states and then performing a PT2 calculation in order to (partly) recover the effect of not using the actual optimal orbitals of each state. The PT2 step also provides an estimate of the dynamical correlation. In fact, it has been shown that the PT2 step provides torsional profiles for the excited state GFP chromophore that differ significantly from those obtained when it is discarded.[8,18,24]

On the other hand, using a three states average (between S_0, S_1, and a third state S_2 involving mainly structure B and, possibly, some Rydberg orbitals) would not be an improvement because the orbitals giving a proper coupling of P and I are not necessarily the same as the orbitals minimizing the energy of S_2. Therefore, the SA2-CAS(4,3)-PT2 method is the best minimal approach.

Energy values from the present quantum calculations (CASSCF and CASPT2 levels) and from other works are given in Table 1 for three critical geometries: TwP, twisted 90° around the phenolic bridge bond (Figure 1); TwI, twisted 90° around the imidazolinone bridge bond; and the hula-twist geometry, twisted 90° around both bonds. Our CASPT2 results are in good agreement with other results at the same level of theory[8,18] (difference smaller than 1 kcal/mol from the highest accuracy results) and differ strongly from our CASSCF results (up to 14 kcal/mol).

Table 1. Energy Differences (in kcal/mol) between Critical Geometries on the S_1 Potential Energy Surface of the Anionic Chromophore (HBI or the Dimethyl Derivative (HBDI) Depending of the Reference) and the Planar cis Fluorescent State (FS) Minimum[a]

	TwP	barrier to TwP	TwI	barrier to TwI	hula-twist
SA2-CAS(4,3)[b]	−14.7		−18.9		−9.2
SA2-CAS(4,3)-PT2[b]	−6.0		−9.7		4.8
Fit $V(\tau,\varphi)$[b]	−6.1	0	−9.8	1	4.8
SA2-CAS(12,11)[c]	−8.6	0	−11.3	0	0.1
SA2-CAS(12,11)-PT2[c]	−7	0	−9	2	4.9
SA2-CAS(2,2)-PT2[d]	−8.8		−5.5		
SA3-CAS(4,3)[e]	−21.5		−28.2		
SA3-CAS(4,3)-PT2[e]	0		−7.2		
SA2-CAS(12,11)[f]	−7	<2	−13	<2	

[a] Definitions of TwP and TwI can be found in Figure 1. $V(\tau,\varphi)$ is the fitting function described in section 2.1. [b] This work. [c] Martin et al.[18] [d] Toniolo et al.[8] [e] Olsen et al.[24] [f] Polyakov et al.[25]

2.2. Fitting Procedure. In the first step of the fitting procedure, before carrying out any parameter optimization, one has to choose a precise definition of the τ and φ variables and their connection with the remaining geometrical variables. It requires to consider several details, and it is presented in Appendix A.

Furthermore, one has to take account of the fact that the τ/φ dependence of the energy in the MD program comes not only from specific dihedral terms but also from van der Waals and electrostatic interactions. We have chosen to adjust the fitting function directly on the CASPT2 energies and to remove the van der Waals and electrostatic interactions that depend on τ and φ when running the MD program (see section 2.3).

In the second step, one has to define a grid of geometries where *ab initio* calculations will be performed. Here, we have used a grid that explores the PES along the two bridge torsion

coordinates with τ and φ frozen at regularly increasing values. Steps of 30° were first used to create a two-dimensional grid of 72 points that covers the complete periods of τ (360°) and φ (180°), and thus the two isomers *cis* (τ = 0°) and *trans* (τ = 180°). We then improved the description of the PES around the planar geometries with a tighter grid of 46 additional calculations for each isomer. Finally, we developed two separate potentials that both cover the complete 2D surface but that have a higher precision for the planar geometry in either the *cis* or the *trans* conformation. In this work, we discuss the dynamics of the *cis* chromophore in GFP and will only detail the *cis* potential.

The 2D grid of CASPT2 energies was interpolated by a sum of products of sine and cosine functions of multiples of τ and φ. The periodicity of 180° for φ was ensured by taking exclusively even multiples of this coordinate (2φ, 4φ, ...). The analytical expression was developed using an iterative procedure that starts with an initial sum of two terms, $\cos(2\varphi)$ and $\cos(2\varphi).\cos(\tau)$, and progressively adds new terms that improve the fit. The new terms are taken from a list of 200 different terms with multiples of τ and φ ranging from 1 to 10. At each iteration, the new terms are tested in order to find the best candidate to add; the relative root-mean-square deviation (rrmsd) of each possible addition is calculated, and the candidate term giving the best improvement of the fit, i.e., resulting in the smallest rrmsd, gets added to the fitting expression. When several terms result in nearly the same value, the term causing the least surface oscillation (evaluated numerically on a tight grid of points) gets selected.

The resulting fitting function $V(\tau,\varphi)$ comprises 30 terms (see the Supporting Information) and reproduces our CASPT2 energy values of the specific geometries, TwI, TwP, and hula-twist, with very good accuracy (differences within 0.1 kcal/mol; Table 1). Heights of the barriers to TwI and TwP are in good agreement with those of other works (differences within 1 kcal/mol). The rrmsd of the fit is 7%.

2.3. Implementation. A new algorithm has been introduced in the Sander module and in the parallel processing PMEMD module of the AMBER program package, allowing the use of a force field including a coupling between two torsion coordinates. A completely new program module was written for the calculation of energies and forces depending on τ and φ. New subroutines were then required for the input and broadcast of (1) potential parameters of $V(\tau,\varphi)$, (2) atom numbers involved in the definitions of the two torsions, and (3) a list of atom pairs whose nonbonded interactions depend on τ and φ.

van der Waals interactions between the atom pairs in this last list were removed by a test function that cross-checks each atom pair treated by the program with this list. A similar test function was used to remove the electrostatic energies between the point charges of atom pairs. Concerning electrostatic interactions, some care has to be exercised to the use of Ewald sums techniques,[29] which consists in evaluating first the electrostatic potential due to all charges of the system and then the energy of each charge in that potential. But, removing the intrachromophore electrostatic energies changes nothing in the potential, and the final electrostatic energy does include all electrostatic interactions between the chromophore and the protein atoms.

2.4. PES Landscape and MD Simulation in vacuo. A two-dimensional representation of $V(\tau,\varphi)$ is shown in Figure 2. It should be emphasized that $V(\tau,\varphi)$ has been obtained via a geometry optimization. It means that all internal coordinates (with the only exception of τ and φ) have been optimized in the excited state. These coordinates include the possible sp^3 hybridization of the imidazolinone bridge bond[8] as well as the Franck−Condon active modes described recently.[30] From the point of view of the fluorescence process, it means that the $\varphi \simeq \tau \simeq 0$ region described by the present potential energy function $V(\tau,\varphi)$ *does not* correspond to the Franck−Condon (FC) region resulting from the vertical transition $S_0 \rightarrow S_1$ but to a region which is reached a very short time after the photon absorption by relaxing internal coordinates, and that is usually called the fluorescent state (FS) [ref 18, Figure 3]. It turns out that indeed one has $\varphi \simeq \tau \simeq 0$ in that region.

The planar FS minimum ($\tau = \varphi = 0°$) lies in the middle of a low-energy valley that comes to a bottleneck at both ends. These narrow exits are reached by a concerted rotation of the bridge bond torsions, $\tau \simeq 30°$ and $\varphi \simeq -30°$ or $\tau \simeq -30°$ and $\varphi \simeq 30°$. In these geometries, the chromophore is at the edge of two

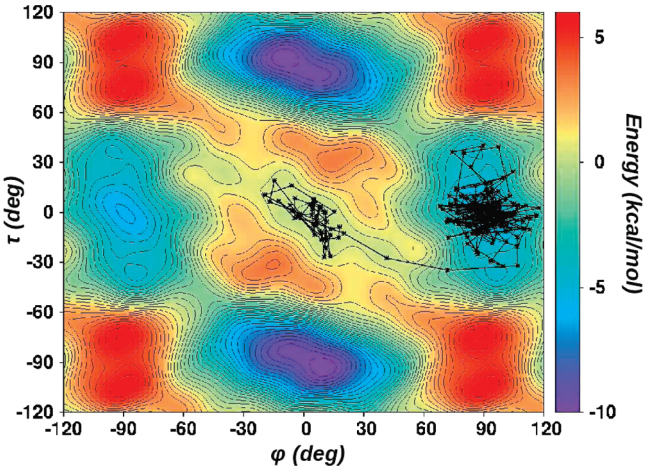

Figure 2. The excited state potential energy surface with a 20 ps trajectory of the anionic chromophore in a vacuum, starting at the planar fluorescent state (FS) minimum ($\tau = \varphi = 0°$). The time step is 1 fs, and coordinates are written out every 0.1 ps.

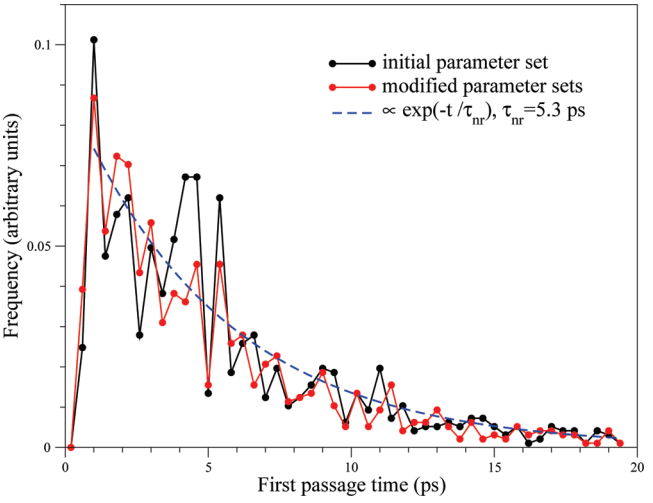

Figure 3. Distributions of first passage times (FPT) at the single-twisted geometries TwP or TwI. A comparison between 1000 simulations with the initial parameter set (solid black line) and 1000 simulations with modified parameter sets (solid red line), see section 2.5. The FPT decay of the initial parameter set is fitted by an exponential (dashed blue line).

potential wells, one that leads to the TwP minimum and one that leads to the TwI minimum, located about 6 and 10 kcal/mol below the FS, respectively. Thus, the minimum energy path involves first concerted variations of φ and τ with opposite signs until $\tau \simeq \pm 30°$ and $\varphi \simeq \mp 30°$ and then a direct downhill motion toward TwP.

All other types of motion are less favorable. A pure φ-twist passes over a 1 kcal/mol barrier and a pure τ-twist over a 2 kcal/mol barrier. In the same way, the path to TwI can be lowered from 2 to 1 kcal/mol by a concerted twist of φ and τ. The geometries where the two rings are perpendicular to each other ($\tau \simeq \pm 45°$, $\varphi \simeq \mp 45°$) lie also about 1 kcal/mol above the FS geometry. The hula-twist maxima (τ and φ close to $\pm 90°$) are located about 5 kcal/mol above FS. The path connecting the planar and these last geometries pass along sharp ridges with steeply sloping sides, leading either to the TwP or to the TwI minima. This result implies that the probability of reaching the hula-twist maxima is low. In addition, it might explain the difficulties reported[18] of finding the MEP between the hula-twist and FS.

Further insight into the PES landscape can be obtained by means of MD simulations of the excited chromophore in vacuo using the torsional potential. We have performed 1000 10-ps-long MD simulations, all starting from a unique planar chromophore structure with randomly generated initial velocities, giving a mean initial kinetic energy of 7.2 ± 1.2 kcal/mol. The anionic chromophore model 4-hydroxybenzylidene-1,2-dimethylimidazolinone (HBDI) was used in these simulations. Details of the force field can be found in Appendix B.

We observed a φ-twist in 90% of the simulations and a τ-twist in the remaining fraction. The preference for the φ-twist is consistent with the barrierless character of this movement. We obtained an exponential distribution of joint first passage times (FPT) at TwP and TwI with a mean value of 5.3 ps. These data are well described by the nonradiative decay $A \exp(-t/\tau_{nr})$, with a nonradiative lifetime of $\tau_{nr} = 5.3$ ps (Figure 3, dashed blue line).

Concerning experimental results on fluorescence in vacuo, a recent work[31] mentions that no fluorescence was detected, and the only quantitative results we can compare to ours come from *ab initio* dynamics[10] using a CASSCF potential that leads to FPT values around 0.5 ps. In the present simulations, less than 1% of the trajectories resulted in a twist within 0.5 ps. The small number of FPTs observed here within the first picosecond is due to the bottleneck profile of the FS valley. The chromophore can only slip through the small exit and reach TwP or TwI in a short period of time if the direction of the randomly generated initial velocities leads directly through the passage. Otherwise, the chromophore will wander within the valley in a random manner until its trajectory finally crosses the exit, and the chromophore can leave the FS valley (Figure 2).

2.5. Assessment and Sensibility of the Fit. In order to assess the fit parameters, we have calculated a new value of the relative root-mean-square deviation, rrmsd, between $V(\tau,\varphi)$ and the CASPT2 values, where the grid point energies were weighted by their visitation frequency in the MD simulations of the chromophore in vacuo. No significant effect was found; the weighted rrmsd was found to be 10% compared to the initial 7%. Thus, it seems that the present fit procedure allows one to reach about the same quality level as what would be obtained by performing the *ab initio* calculations on the fly along dynamics while retaining a systematic and computer-time-saving character.

In addition, the accuracy of the predictions obtained by MD simulations was tested by evaluating their dependence on small variations of the parameters. To that end, the distribution of FPTs obtained with the initial parameters was compared to a distribution resulting from 1000 new simulations obtained by randomly modified parameters. The modifications were chosen in order to reflect the uncertainty of the parameters corresponding to the uncertainty of the fit. They were obtained according to normal distributions whose centers are on the initial parameter values, and the standard deviation σ_k of parameter k is given by (ref 34, eq 15.6.4)

$$\sigma_k^2 = \frac{\chi^2}{C_{kk}}$$

where C_{kk} is the diagonal element of the covariant matrix of the fit functions and χ is the root-mean-square deviation. This expression makes sense only if the covariant matrix is diagonal, and we applied it to unitary combinations of parameters that diagonalize that matrix. In addition, we applied two constraints that locate a minimum at the planar geometry in the potentials resulting from the varied parameters.

The two resulting FPT distributions, either from the initial parameter set or from the 1000 modified parameter sets can be seen in Figure 3. The shift in the median, caused by the parameter modifications, is small (0.4 ps) and not significant compared to the width of the 50% confidence interval (centered on the median) of the two distributions (5 ps). We conclude that the present fit can be used safely to evaluate the fluorescent lifetime.

3. MD SIMULATIONS AND FLUORESCENCE LIFETIME OF GFP

In the present MD simulations, we have chosen to neglect the polarization of the electronic wave function of the chromophore by the protein environment. The polarization effect has been shown to be important in water[8,9,35] and to significantly accelerate the torsion dynamics compared to the isolated chromophore.[8,9] However, the proteic environment is generally less polar than bulk water and would not influence the chromophore behavior as much. Indeed, the experimental absorption maximum wavelength of the anionic chromophore in water,[36] in vacuo,[37] and in wt-GFP[38] is found at 426 nm, ~475 nm, and 475 nm, respectively. It suggests a weak influence of the protein matrix in near-planar geometries, but one cannot rule out a larger effect on twisted geometries like the hula-twist. Nevertheless, the method used here is a reasonable compromise between accuracy and feasibility. It allows one to carry out nanoseconds-long MD of the protein with a simple force field that captures the main features of the torsional landscape of the excited chromophore.

We have performed 24 MD simulations of the excited state of the S65T mutant of green fluorescent protein (S65T-GFP) in which the chromophore is known to be essentially in its anionic form.[39] All excited state simulations started from structures randomly extracted from a ground state simulation of the protein and had a total time duration of 15 ns; further details are given in Appendices B and C. We observed a 90° twist around φ within a few nanoseconds (0.2−12.9 ns) in all simulations, but no 90° twist around τ, a result that can be related to the larger sweep of the conformational space than the one involved in other rotations. The mean first passage time (MFPT) at TwP was 4.0 ns. Concerning the hula-twist geometry, it is not visited in any of the 24 trajectories, consistently with its high energy (5 kcal/mol above FS).

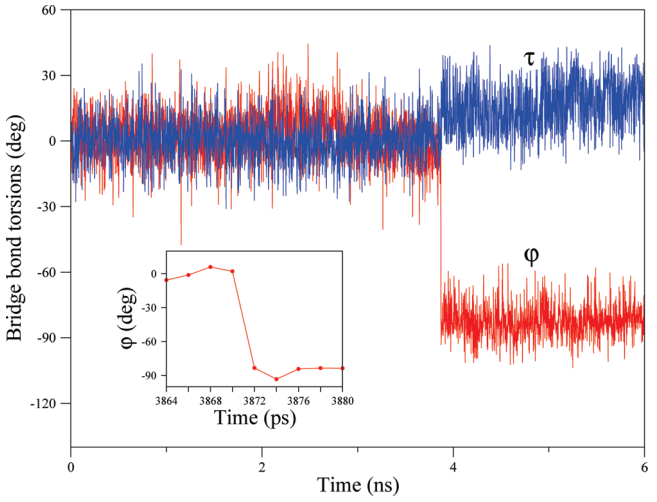

Figure 4. Bridge bond torsions (τ and φ) from an excited state MD simulation of the solvated GFP with the anionic chromophore. Snapshots were taken every 2 ps. The inset presents a zoom on the time window where the φ twist occurs.

A striking aspect of the observed twist is that, in all cases, it occurs suddenly: the values of φ and τ oscillate around 0° for a while, and then, at a given time, the value of φ switches from about 0° to about −90° within a time interval shorter than 5 ps, while τ slightly increases. This behavior of φ is illustrated in Figure 4 for one of the simulations. The time of 5 ps required by the φ-twist is to be compared to the MFPT found in vacuo (5.3 ps). The sudden character of the rotation and the time it requires suggest a description of the interplay between the chromophore and the protein dynamics: in the excited state, the chromophore twists within a few picoseconds in vacuo, but, in the protein, the pocket surrounding the chromophore is too small and the twist is hindered most of the time. However, there are some collective motions of the protein with a long periodicity (several nanoseconds) which modify the pocket and relax the constraint: in such cases, the chromophore dynamics becomes the same as that in vacuo, and the twist occurs within a few picoseconds.

For the time being, this description is just a hypothesis, and in order to verify it, it would be useful to identify the very low frequency motion of the protein in the microwave domain responsible for the constraint removal. That hypothesis suggests that the fluorescence properties of the FPs depend not only on the type and strength of the anchoring of the chromophore in its pocket but also on the nature of the low frequency collective motions (which might be related to the β-barrel structure).

We now look for an evaluation of the nonradiative decay rate of S65T-GFP arising from our results. To that end, we need quantitative information about the link between the twist movement of the excited chromophore and the fluorescence quenching. The process usually invoked for fluorescence quenching of GFP's chromophores is a nonradiative relaxation to the ground state by internal conversion or through a conical intersection, occurring *via* the twisted geometries. But, in fact, the oscillator strengths of the transition S_0-S_1 have been found to be totally cancelled (ref 24, Table 1) in the twisted geometries TwP and TwI. Thus, whatever the fate of the chromophore once it reaches the TwP geometry, the fluorescence emission is immediately quenched.

Table 2. Theoretical versus Experimental Lifetimes (ns) and Quantum Yield of S65T-GFP[a]

	this work	experiment
fluorescence lifetime τ_{fluo}	2.20	3.01[b]
radiative lifetime τ_r		4.7
non radiative lifetime τ_{nr}	4.0	8.3
quantum yield ϕ	0.46	0.64[c]

[a] The theoretical τ_{nr} is obtained directly from the MD simulations; the experimental τ_r and τ_{nr} are deduced from the experimental τ_{fluo} and ϕ, according to eq 1; the theoretical τ_{fluo} is deduced from the theoretical τ_{nr} and the experimental τ_r using eqs 2. [b] Volkmer et al.[40] [c] Patterson et al.[38]

Consequently, the fluorescence lifetime τ_{fluo} has to be distinguished here from the excited state lifetime τ_{S1}. The latter has been evaluated by multiple spawning AIMS (ref 10, Supporting Information, Figure S1.7): it has been found that the fluorescence is quenched by a 90° φ-twist within 0.3 ps but that only 2% of the ground state population is recovered within the total simulation time of 0.5 ps (average over 15 trajectories), giving rise to an excited state lifetime on the order of 25 ps. The experimentally observable quantity τ_{fluo} is thus different from τ_{S_1}. The two lifetimes are identical only if all excited state geometries can deactivate by green fluorescence emission. Therefore, the observed quantum yield should be written here as

$$\phi = \frac{\tau_{fluo}}{\tau_r} \quad (1)$$

(where τ_r is the radiative lifetime) instead of the usual $\phi = \tau_{S_1}/\tau_r$ (see, for instance, ref 32, eq 3.11; ref 33, eq 1.5).

Similarly, one has to use

$$\frac{1}{\tau_{fluo}} = \frac{1}{\tau_r} + \frac{1}{\tau_{nr}} \quad (2)$$

instead of the usual $1/\tau_{S_1} = 1/\tau_r + 1/\tau_{nr}$ (ref 32, eq 3.3).

When substituting the experimental values of ϕ and of τ_{fluo} into eqs 1 and 2, one gets an estimate of the experimental value of τ_{nr}. According to the analysis above, that value should be compared with the MFPT resulting from the MD simulations rather than with the excited state lifetime.

Results are shown in Table 2. It appears that our MD simulations underestimate τ_{nr} by approximately 4 ns (50%). Theoretical values of τ_{fluo} and ϕ can be evaluated by combining the theoretical nonradiative lifetime and the experimental radiative lifetime. One obtains 2.2 ns for τ_{fluo} and 0.46 for ϕ, in qualitative agreement with experimental values (3.0 ns and 0.64, respectively). To the best of our knowledge, this is the first theoretical evaluation of the fluorescence lifetime and quantum yield of a fluorescent protein. The radiative lifetime is a characteristic property of a given chromophore, that is only weakly dependent on the environment.[41] As it should remain rather similar for GFP variants differing only by a few mutations, the methods developed here may help in predicting their relative brightness through MD simulations.

We conclude that our method is able to predict the right order of magnitude of the fluorescent lifetime. Yet, it is useful to investigate the origin of the difference between our result and the experimental values. In this respect, one first points out the small number (24) of FPTs that are used for deducing the MFPT. Could we expect a better agreement by using more FPT values?

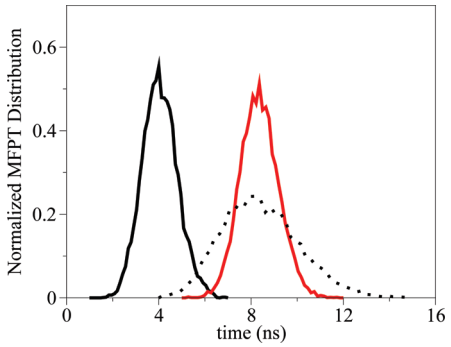

Figure 5. MFPT distribution F_{sim} from Bootstrap-treated MD results (solid black line). MFPT distribution F_{exp} (n = 100) from random draws of 100 FPT values extracted from the nonradiative decay distribution ($\exp(-t/\tau_{nr})$ with τ_{nr} = 8.3 ns; solid red line). MFPT distribution F_{exp} (n = 24) from random draws of 24 FPT values from the nonradiative decay distribution (dotted black line).

In order to tackle that question, we have assumed that our 24 FPTs can be considered as 24 draws of a random variable with an exponential probability distribution f_{sim} and an unknown decay constant. One can then try to compare the resulting MFPT with what would be obtained using the distribution deduced from experimental results: $f_{exp}(\mathrm{FPT}) = \exp(-\mathrm{FPT}/\tau_{nr})$ with τ_{nr} = 8.3 ns (Table 2). That comparison can be made indirectly by first resampling our 24 values using the bootstrap techniques,[42] giving a distribution F_{sim} of MFPTs: that distribution F_{sim} mimics what would be obtained if more than 24 simulations were available and distributed into N bundles of 24 simulations each in order to get a distribution of N values of MFPT. Thus, F_{sim} can be compared with the distribution F_{exp} obtained by using a large number N (= 1000) of sets of n = 24 draws according to f_{exp}, each set giving a value of MFPT. In fact, we have determined two distributions F_{exp}, one distribution using n = 24 and the other using n = 100. The results are shown in Figure 5.

We first observe in Figure 5 that the two F_{exp} distributions are centered close to the exact limit value, 8.3 ns. It means that 24 draws of FPT from an exponential distribution like f_{sim} also should result in a distribution of MFPT centered close to the exact limit value obtained if $n \rightarrow \infty$. Therefore, that limit is closer to 4.0 ns than to 8.3 ns, and one has to look for another origin of this difference between the theoretical and experimental τ_{nr} than the small number of FPTs available here.

A possible reason might come from the force field parameters used here: if the protein is too flexible and/or the anchoring of the chromophore is too weak, one probably gets a MFPT which is too short, as found here. Another possible origin can lie in the choice of the 24 initial geometries for the simulations of the excited state. They have been extracted from a 5-ns-long simulation of the ground state, which could be too short to trigger all of the appropriate modes of the protein that can relax or hinder the chromophore twist.

These tracks will be pursued in future works. Despite these limitations, this work offers the first precise representation of the excited chromophore PES and gives access to realistic and unbiased dynamics of excited FPs on a long time scale.

4. CONCLUSION

We have determined a coupled torsional potential $V(\tau,\varphi)$ for the S_1 state of the anionic chromophore of the green fluorescent protein (GFP), by fitting a grid of SA2-CAS(4,3)-PT2 energy values, and implemented this potential in the parallel module PMEMD of the AMBER package. Using this new program, we have run 24 long trajectories (15-ns-long each) of the brightly fluorescent S65T-GFP. It is the first time to our knowledge that such long free simulations have been carried out for a fluorescent protein with the chromophore in the excited state. We observed a mean first passage time at the φ twisted geometry of 4 ns, which corresponds to a fluorescence lifetime around 2 ns and a quantum yield around 0.5, in qualitative agreement with the experimental data. It appears from these trajectories that the twist movement is very fast once the chromophore leaves the fluorescent state valley, suggesting that it happens when collective motions of the protein allow the chromophore to move in its pocket.

The new tool presented in this work is complementary to the already existing QM/MD methods applied for the study of chromophores in a vacuum or solution, or in weakly fluorescent proteins with a fluorescence lifetime on the picosecond time scale. It is likely to suffer from limitations inherent in the use of classical force fields, which does not take into account the polarization effect between the chromophore and the proteic environment. However, it captures the main features of the torsional behavior of the S_1 state and leads to satisfactory results for S65T-GFP. Applied to other FPs it should be able to provide the right order of magnitude of the nonradiative lifetime τ_{nr}. Since quantum yield values such as 0.6, 0.1, and 0.001 correspond to different orders of magnitude of τ_{nr} ($\approx$ 7, 0.5, and 0.005 ns, respectively), it should allow one to unambiguously distinguish proteins with bright, moderate, or very weak fluorescence and to provide analyses of the structural and dynamical factors responsible for these differences.

APPENDICES

Appendix A. Choice of Coordinates. There are two technical difficulties in defining and using the two variables τ and φ of the present 2D potential.

First, each torsion coordinate τ and φ can be described by four dihedral angles, and these angles usually have different values after geometry optimization as well as along the MD calculation.

Second, the equilibrium angles along the bridge depend on τ and φ. Particularly, they take larger values near planar geometries than for twisted geometries, to avoid a close approach of O2 or N2 (on the imidazolinone ring) to HD1 (the H atom linked to CD1 on the phenolate ring); see Figure 6.

We have adopted the following protocol in order to fix these two types of problems:

In geometry optimizations of the S_1 state, the points of the grid (τ, φ) have been defined by fixing the values of two dihedral angles, τ_C = C2−CA2−CB2−CG2 and φ_1 = CA2−CB2−CG2−CD1; the other dihedral angles around the CA2−CB2 and CB2−CG2 bonds were let free. The resulting geometry is then labeled by τ and φ values defined through the following expressions: $\tau = (\tau_c + \tau_N - 180°)/2$ with τ_N = N2−CA2−CB2−CG2 and $\varphi = (\varphi_1 + \varphi_2 - 180°)/2$ with φ_2 = CA2−CB2−CG2−CD2. The energy of the optimized geometry is ascribed to the resulting τ and φ values in the fit procedure. Then, in MD simulation, we have calculated $V(\tau,\varphi)$ and the torsional forces using the values of the dihedral angles (τ_N or τ_C, φ_1 or φ_2) as torsion τ/φ coordinates. The four values $V(\tau,\varphi)$ obtained in this way are usually different, and the average is finally used.

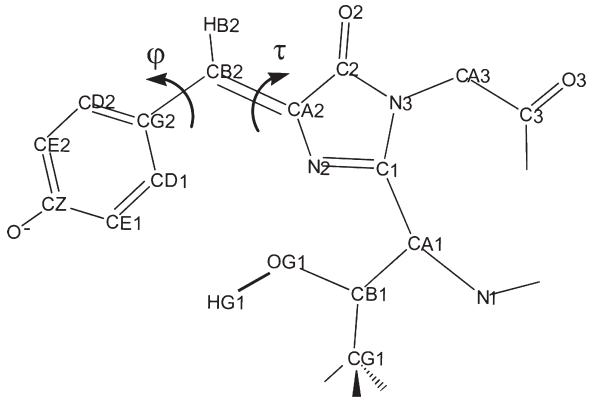

Figure 6. Anionic chromophore of S65T-GFP including the links to the α helix. Atom labels are taken from the Protein Data Bank (entry 1EMA) with the exception of the phenolate oxygen.

Concerning the bridge angles, we use an average of the planar and twisted optimized values.

Appendix B. Force Field. The AMBER 1999 force field, "ff99", was used for all standard amino acids.

Concerning the chromophore, atomic charges were derived from the *ab initio* molecular potential calculated at the RHF/6-31G* level for the electronic ground state and CIS/6-31G* for the excited state, in the corresponding optimized planar *cis* geometries. Concerning the simulations of GFP, the chromophore model used for these calculations includes the two peptide links to the protein. Several constraints were imposed in the fitting procedure, using a program developed by two of us:[43] the total charge of the atoms capping the chromophore was constrained to zero and the charges of those involved in the two peptide bonds were constrained to their values in the AMBER force field. Harmonic constraints were set on the atoms of the Thr65 and Gly67 parts, with target values taken from the AMBER force field. Weak harmonic constraints with target values set to zero were applied to all other atoms in order to avoid large unphysical values. The resulting values are shown in the Supporting Information.

As concerns the τ,φ torsional potential, the coupled potential developed in this work was used for the excited state simulations. Concerning the ground state simulation, where the chromophore never explores strongly twisted geometries, we have assumed that the coupling between the two torsions could be neglected and used the independent τ and φ potentials of Reuter et al.[44] Concerning the other bonded terms, equilibrium values involved in the bridge and the imidazolinone ring were taken from the *ab initio* optimized planar *cis* geometries. The remaining equilibrium values and all force constant values were chosen by analogy with similar chemical situations in the AMBER force field. An exception concerns the bond angles involving the bridging bonds in the excited state, which were taken as the average of the planar and twisted geometries values (see Appendix A).

Appendix C. Molecular Dynamics Details. The starting coordinates were taken from the crystal structure of S65T-GFP, in which the chromophore is known to be essentially in its anionic form (Protein Data Bank entry 1EMA).[39] The protonation states of the histidine residues were assigned as described in the work of Helms et al.[45] Glu222 was taken in its protonated (neutral) form.[46] Molecular dynamics (MD) simulations were carried out using the AMBER 10 suite.[20] Hydrogen atoms, water molecules, and neutralizing ions were added using the LEaP program. An initial minimization of the energy of the system was followed by an equilibration procedure consisting of a constant-volume simulation where the temperature was raised gradually from 100 to 300 K and then by a constant-pressure simulation. In order to avoid large conformational changes, the protein was constrained by weak harmonic forces (force constant = 5 kcal mol $^{-1}$ Å $^{-1}$) during equilibration. The constraints were then gradually removed, and the equilibration procedure was completed by a unconstrained MD simulation of 1 ns. Periodic boundary conditions were used, and the particle-mesh Ewald method[29] was used to handle the electrostatic interactions. The cutoff for the van der Waals interactions and for the direct part of the electrostatic interactions was set to 10 Å.

A 5-ns-long MD simulation, with the chromophore in its electronic ground state, was then run in order to obtain initial coordinates for the excited state simulations. Finally, several 15-ns-long MD simulations, with the chromophore in its electronic excited state, were run with starting coordinates taken among these snapshots. The MD simulations were run in the NPT ensemble, using a time step of 2 fs and with snapshots saved every 2 ps.

■ ASSOCIATED CONTENT

Supporting Information. Three pages containing the complete analytical expression of the 2D potential and atomic point charges used in MD simulations. This information is available free of charge via the Internet at http://pubs.acs.org.

■ AUTHOR INFORMATION

Corresponding Author

*E-mail: gabriella.jonasson@u-psud.fr, isabelle.demachy@u-psud.fr.

■ ACKNOWLEDGMENT

We thank Pascal Pernot and Hélène Pasquier for helpful discussions. We are also grateful to all members of the experimental-theoretical collaboration in the photophysics of fluorescent proteins at Laboratoire de Chimie Physique. This work was granted access to the HPC resources of CINES under the allocation 2010-[c2010086318] made by GENCI (Grand Equipement National de Calcul Intensif). We also acknowledge the use of the cluster computing facility available at Laboratoire de Chimie Physique.

■ REFERENCES

(1) Tsien, R. Y. *Annu. Rev. Biochem.* **1998**, *67*, 509–544.
(2) Zimmer, M. *Chem. Rev.* **2002**, *102*, 759–781.
(3) Chudakov, D. M.; Lukyanov, S.; Lukyanov, K. A. *Trends Biotechnology* **2005**, *23*, 605–613.
(4) Wachter, R. M. *Photochem. Photobiol.* **2006**, *82*, 339–344.
(5) Day, R. D.; Davidson, M. W. *Chem. Soc. Rev.* **2009**, *38*, 2887–2921.
(6) Mandal, D.; Tahara, T.; Meech, S. R. *J. Phys. Chem. B* **2004**, *108*, 1102–1108.
(7) Merola, F.; Levy, B.; Demachy, I.; Pasquier, H. Photophysics and Spectroscopy of Fluorophores in the Green Fluorescent Protein Family. In *Advanced Fluorescence Reporters in Chemistry and Biology I: Fundamentals and Molecular Design, Springer Series on Fluorescence*, 1st ed.; Demchenko, A. P., Ed.; Springer: Berlin, 2010; Vol. 8, pp 347−383.

(8) Toniolo, A.; Olsen, S.; Manohar, L.; Martinez, T. J. *Faraday Discuss.* **2004**, *127*, 149–163.
(9) Virshup, A. M.; Punwong, C.; Pogorelov, T. V.; Lindquist, B. A.; Ko, C.; Martinez, T. J. *J. Phys. Chem. B* **2009**, *113*, 3280–3291.
(10) Olsen, S.; Lamothe, K.; Martinez, T. J. *J. Am. Chem. Soc.* **2010**, *132*, 1192–1193.
(11) Maddalo, S. L.; Zimmer, M. *Photochem. Photobiol.* **2006**, *82*, 367–372.
(12) Megley, C. M.; Dickson, L. A.; Maddalo, S. L.; Chandler, G. J.; Zimmer, M. *J. Phys. Chem. B* **2009**, *113*, 302–308.
(13) Moors, S. L. C.; Michielssens, S.; Flors, C.; Dedecker, P.; Hofkens, J.; Ceulemans, A. *J. Chem. Theory Comput.* **2008**, *6*, 1012–1020.
(14) Vallverdu, G.; Demachy, I.; Ridard, J.; Lévy, B. *THEOCHEM* **2009**, *898*, 73–83.
(15) Schäfer, L. V.; Groenhof, G.; Boggio-Pasqua, M.; Robb, M. A.; Grubmüller, H. *PLoS Comput. Biol.* **2008**, *4*, e1000034.
(16) Li, X.; Chung, L. W.; Mizuno, H.; Miyawaki, A.; Morokuma, K. *J. Phys. Chem. Lett.* **2010**, *1*, 3328–3333.
(17) Liu, R. S. H.; Browne, D. T. *Acc. Chem. Res.* **1986**, *19*, 42–48.
(18) Martin, M. E.; Negri, F.; Olivucci, M. *J. Am. Chem. Soc.* **2004**, *126*, 5452–5464.
(19) Olsen, S.; McKenzie, R. *J. Chem. Phys.* **2009**, *130*, 184302.
(20) Case, D. A.; Darden, T. A.; Cheatham, T. E., III; Simmerling, C. L.; Wang, J.; Duke, R. E.; Luo, R.; Crowley, M.; Walker, R. C.; Zhang, W.; Merz, K. M.; Wang, B.; Hayik, S.; Roitberg, A.; Seabra, G. Kolossváry, I.; Wong, K. F.; Paesani, F.; Vanicek, J.; Wu, X.; Brozell, S. R.; Steinbrecher, T.; Gohlke, H.; Yang, L.; Tan, C.; Mongan, J.; Hornak, V.; Cui, G.; Mathews, D. H.; Seetin, M. G.; Sagui, C.; Babin, V.; Kollman, P. A. *AMBER 10*; University of California: San Francisco, CA, 2008.
(21) Roos, B. O.; Taylor, P. R.; Siegbahn, P. E. M. *Chem. Phys.* **1980**, *48*, 157.
(22) Frisch, M. J.; Trucks, G. W.; Schlegel, H. B.; Scuseria, G. E.; Robb, M. A.; Cheeseman, J. R.; Montgomery, J. A., Jr.; Vreven, T.; Kudin, K. N.; Burant, J. C.; Millam, J. M.; Iyengar, S. S.; Tomasi, J.; Barone, V.; Mennucci, B.; Cossi, M.; Scalmani, G.; Rega, N.; Petersson, G. A.; Nakatsuji, H.; Hada, M.; Ehara, M.; Toyota, K.; Fukuda, R.; Hasegawa, J.; Ishida, M.; Nakajima, T.; Honda, Y.; Kitao, O.; Nakai, H.; Klene, M.; Li, X.; Knox, J. E.; Hratchian, H. P.; Cross, J. B.; Bakken, V.; Adamo, C.; Jaramillo, J.; Gomperts, R.; Stratmann, R. E.; Yazyev, O.; Austin, A. J.; Cammi, R.; Pomelli, C.; Ochterski, J. W.; Ayala, P. Y.; Morokuma, K.; Voth, G. A.; Salvador, P.; Dannenberg, J. J.; Zakrzewski, V. G.; Dapprich, S.; Daniels, A. D.; Strain, M. C.; Farkas, O.; Malick, D. K.; Rabuck, A. D.; Raghavachari, K.; Foresman, J. B.; Ortiz, J. V.; Cui, Q.; Baboul, A. G.; Clifford, S.; Cioslowski, J.; Stefanov, B. B.; Liu, G.; Liashenko, A.; Piskorz, P.; Komaromi, I.; Martin, R. L.; Fox, D. J.; Keith, T.; Al-Laham, M. A.; Peng, C. Y.; Nanayakkara, A.; Challacombe, M.; Gill, P. M. W.; Johnson, B.; Chen, W.; Wong, M. W.; Gonzalez, C.; Pople, J. A. *Gaussian 03*, Revision C.02; Gaussian, Inc.: Wallingford, CT, 2004.
(23) Werner, H.-J.; Knowles, P. J.; Manby, F. R.; Schütz, M.; Celani, P.; Knizia, G.; Korona, T.; Lindh, R.; Mitrushenkov, A.; Rauhut, G.; Adler, T. B.; Amos, R. D.; Bernhardsson, A.; Berning, A.; Cooper, D. L.; Deegan, M. J. O.; Dobbyn, A. J.; Eckert, F.; Goll, E.; Hampel, C.; Hesselmann, A.; Hetzer, G.; Hrenar, T.; Jansen, G.; Koppl, C.; Liu, Y.; Lloyd, A. W.; Mata, R. A.; May, A. J.; McNicholas, S. J.; Meyer, W.; Mura, M. E.; Nicklass, A.; Palmieri, P.; Pflüger, K.; Pitzer, R.; Reiher, M.; Shiozaki, T.; Stoll, H.; Stone, A. J.; Tarroni, R.; Thorsteinsson, T.; Wang, M.; Wolf, A. *MOLPRO*, version 2006.1; University College Cardiff Consultants Limited: Cardiff, Wales, 2010.
(24) Olsen, S.; Smith, S. C. *J. Am. Chem. Soc.* **2008**, *130*, 8677–8689.
(25) Polyakov, I. V.; Grigorenko, B. L.; Epifanovsky, E. M.; Krylov, A. I.; Nemukhin, A. V. *J. Chem. Theory Comput.* **2010**, *6*, 2377–2387.
(26) Shapiro, I.; Ryazantsev, M. N.; Ding, W. J.; Huntress, M. M.; Melaccio, F.; Andruniow, T.; Ollivucci, M. *Aust. J. Chem.* **2010**, *63*, 413–429.
(27) Braida, B.; Walter, C.; Engels, B.; Hiberty, P. C. *J. Am. Chem. Soc.* **2010**, *132*, 7631–7637.
(28) Olsen, S. *J. Chem. Theory Comput.* **2010**, *6*, 1089–1103.
(29) Darden, T.; York, D.; Pedersen, L. *J. Chem. Phys.* **1993**, *98*, 10089–10092.
(30) Kamarchik, E.; Krylov, A. I. *J. Phys. Chem. Lett.* **2011**, *2*, 488–492.
(31) Forbes, M. W.; Joskusch, R. A. *J. Am. Chem. Soc.* **2009**, *131*, 17038–17039.
(32) Valeur, B. Characteristics of fluorescence emission. In *Molecular Fluorescence*, 1st ed.; Valeur, B., Ed.; Wiley-VCH: Weinheim, Germany, 2002; pp 46−47.
(33) Lakowitz, J. R. Introduction to fluorescence. In *Principles of Fluorescence Spectroscopy*, 2nd ed.; Lakowitz, J. R., Ed.; Kluwer Academic/Plenum Publishers, New York, 1999; pp 10−11.
(34) Press, W. H.; Teukolsky, S. A.; Vetterling, W. T.; Flannery, B. P. Modeling of Data. In *Numerical Recipes in FORTRAN: The Art of Scientific Computing*, 2nd ed.; Press, W. H., Teukolsky, S. A., Vetterling, W. T., Flannery, B. P., Eds.; Cambridge University Press: New York, 1992: pp 690−691.
(35) Altoe, P.; Bernardi, F.; Garavelli, M.; Orlandi, G.; Negri, F. *J. Am. Chem. Soc.* **2005**, *127*, 3952–3963.
(36) Dong, J.; Solntsev, K. M.; Tolbert, L. M. *J. Am. Chem. Soc.* **2006**, *128*, 12038–12039.
(37) Nielsen, S. B.; Lapierre, A.; Andersen, J. U.; Pedersen, U. V.; Tomita, S.; Andersen, L. H. *Phys. Rev. Lett.* **2001**, *87*, 228102.
(38) Patterson, G. H.; Knobel, S. M.; Sharif, W. D.; Kain, S. R.; Piston, D. W. *Biophys. J.* **1997**, *73*, 2782–2790.
(39) Ormö, M.; Cubitt, A. B.; Kallio, K.; Gross, L. A.; Tsien, R. Y.; Remington, S. J. *Science* **1996**, *273*, 1392–1395.
(40) Volkmer, A.; Subramaniam, V.; Birch, D. J. S.; Jovin, T. M. *Biophys. J.* **2000**, *78*, 1589–1598.
(41) Strickler, S. J.; Berg, R. A. *J. Chem. Phys.* **1962**, *37*, 814–822.
(42) Efron, B. *Ann. Stat.* **1979**, *7*, 1–26.
(43) Ridard, J.; Lévy, B. *J. Comput. Chem.* **1999**, *20*, 473–482.
(44) Reuter, N.; Lin, H.; Thiel, W. *J. Phys. Chem. B* **2002**, *106*, 6310–6321.
(45) Helms, V.; Straatsma, T. P.; McCammon, J. A. *J. Phys. Chem. B* **1999**, *103*, 3263–3269.
(46) Nifosi, R.; Tozzini, V. *Proteins: Struct., Funct. Genet.* **2003**, *51*, 378–389.